DOI: 10.1002/smll.201802328
Article type: Full Paper

A literal elytral rainbow: Tunable structural colors using single diamond biophotonic crystals in *Pachyrrhynchus congestus* weevils

Bodo D. Wilts[1,], and Vinodkumar Saranathan[2-5,]**

Dr. B. D. Wilts
[1] Adolphe Merkle Institute, University of Fribourg, Chemin des Verdiers 4, 1700 Fribourg, Switzerland
E-mail: bodo.wilts@unifr.ch

Dr. V. Saranathan
[2] Division of Science, Yale-NUS College, 10 College Avenue West, 138609, Singapore.
[3] NUS Nanotechnology and Nanoscience Initiative (NUSNNI-NanoCore), National University of Singapore, 117576, Singapore.
[4] Department of Biological Science, National University of Singapore, 117543, Singapore.
[5] Lee Kong Chian Natural History Museum, National University of Singapore, 117377, Singapore.
E-mail: vinodkumar.saranathan@aya.yale.edu

Keywords: biophotonics, tunable colors, single diamond biophotonic crystals, structurally colored weevils, iridescent biological displays

The brilliant colors of many insects arise from the interference of incident light with complex nanostructured biomaterials that are present in their cuticle. Here, we investigate the rainbow-colored spots on the elytra of a snout weevil, *Pachyrrhynchus congestus pavonius* (Coleoptera: Curculionidae) using synchrotron small-angle x-ray scattering (SAXS), scanning electron microscopy, microspectrophotometry and photonic bandgap modeling. We show that the iridescent scales present in the rainbow-hued spots are due to a 3D photonic crystal network of chitin in air with a single diamond (*Fd*-3*m*) symmetry. In many insects, different orientations of photonic crystal domains are used to create various hues. In this weevil, however, both the chitin volume fractions as well as the lattice parameters of the biologically self-assembled single diamond nanostructure are

varied to achieve the remarkable tuning of the structural colors across the visible light spectrum on a scale-by-scale basis. Uncovering the precise mechanism of color tuning employed by this weevil has important implications for further structural and developmental research on biophotonic nanostructures and may provide fresh impetus for bio-inspired and biomimetic multi-functional applications, as synthesis of photonic crystals at visible length scales is currently challenging.

1. Introduction

The vivid, iridescent organismal displays in nature, *e.g.*, those of many beetles, butterflies, birds, fishes, and cephalopods, are due to interference of light scattered by nanostructured biomaterials present in the integument [1-8]. When the refractive index (RI) or the material makeup of the integument varies periodically or quasi-periodically on the length scale of about half of the visible light wavelengths (~150-300 nm) in one, two or all three dimensions, the resulting crystalline or amorphous photonic nanostructures act as interference reflectors of light, with iridescent or isotropic optical properties, respectively [9-12]. Of great fundamental and applied interest to the physics and engineering community currently are three-dimensional photonic crystals (3DPCs) with single diamond (*Fd*-3*m*) and single gyroid ($I4_132$) symmetries that are based on Schwartz's Diamond (*D*) and Schoen's Gyroid (*G*) triply periodic minimal surfaces (TPMS), respectively [13-22]. The single gyroid and single diamond PCs can exhibit full or complete photonic bandgaps (PBGs) in contrast to their corresponding double symmetries (the double diamond *Pn*-3*m* and double gyroid *Ia*-3*d*) that feature only partial or pseudo bandgaps. In particular, single diamond PCs are known to possess the largest full photonic bandgaps, compared to any other photonic nanostructure [14, 15]. Although the double diamond and double gyroid morphologies can be realized experimentally using bottom-up self-assembly of block polymers, and can be selectively etched to remove one of or more

(matrix or network) phases, to our knowledge, there is no direct route to self-assembling single diamond and single gyroid network phases, let alone at the optically relevant meso-scale (150-300 nm) [21-30]. Other approaches aimed at synthesizing these network phase 3DPCs include laser lithography [31, 32] and sol-gel replication of insect photonic scales with various degrees of success [33, 34], although routine synthesis at optical length scales remains a considerable challenge.

Many of the naturally occurring biophotonic nanostructures, however, appear to be rather facilely self-assembled within the cells of the developing organism [35-43]. In particular, iridescent scales from many land arthropods (insects, spiders and tarantulas) have been recently diagnosed to possess biophotonic nanostructures spanning the amphiphilic or lyotropic phase space, *i.e.*, they exhibit biophotonic analogs of all the morphologies commonly seen during the phase behavior of block polymer melts, lipid-water or surfactant mixtures (that have length scales on the order of tens of nm), but at the much harder to achieve optical length scales [38, 42, 44, 45]. These nanostructures appear to be templated *in vivo* by the complex folding of biological membranes and the deposition of chitin, followed by programmed cell death to leave behind solid, chitinous biophotonic nanostructures in air [36, 38, 42, 43, 45]. Moreover, given the low RIs of the biological materials employed in biophotonic nanostructures (ranging from ~1.3 to ~1.9, [46, 47]; although, some higher RI materials are known, with values ~2.4 [48]), many recent studies have shown that their optical reflectance properties have become nearly optimal over the course of evolution [21, 49-54]. These results underscore the importance of these 3DPCs for bioinspiration and biomimetics for a variety of multi-functional applications [55-57].

In the insect order Coleoptera (beetles and weevils), a large diversity of biophotonic nanostructures has been observed [reviewed in 45, 58]. For example, many beetles have multilayers in the cuticle of the elytra (modified forewings that serve as protective hindwing cases) and body, making them highly reflective [59]. In scarab beetles, a plywood-like

helicoidally layered cuticle in the elytra cause bright circularly polarized reflections [60, 61]. Even more sophisticated 3DPCs exist in snout weevils, including the single diamond and single gyroid network morphologies [42, 44, 45, 58, 62, 63]. One such intriguing snout weevil found in Philippines with remarkable structural coloration is *Pachyrrhynchus congestus pavonius* (Heller 1921, Coleoptera: Curculionidae: Entiminae: Pachyrhynchini), which has rainbow colored spots on their elytra (**Figure 1**). These spots are comprised of concentric rings of nearly circular scales that vary in color from red, orange, yellow, green, cyan to blue hues (going radially inwards), essentially similar to the color sequence of a rainbow (ROYGB). The coloration in this taxon (or likely a variety of this subspecies) was previously investigated by Welch and coworkers [64] using scanning electron microscopy (SEM) and transfer-matrix optical modelling. The authors exclusively investigated the "orange" scales of the multi-colored spots and concluded that the nanostructure is an opal-like polycrystal assembly with face-centered cubic (*f.c.c.*) symmetry [64], when such an opal nanostructure is unknown among other closely related Pachyrrhynchine weevils [42, 44, 45]. Using Small-Angle X-ray Scattering (SAXS), Scanning Electron Microscopy (SEM), microspectrophotometry and PBG modelling, we revisit this weevil here with the goal of accurately diagnosing the 3DPCs in the iridescent scales and interrogating the precise mechanism of color tuning employed by this weevil to create this literal elytral rainbow.

2. Results

2.1. Overall appearance

P. c. pavonius is a dark, glossy weevil with a slight maroon tinge and bears highly conspicuous annular or concentric spots on the dorsal and lateral sides of its thorax and abdomen (on the elytra). These multi-colored annular rings feature violet/deep blue scales at the center that gradually grade away on a scale-by-scale basis to orange or red hues on the outer perimeter

(Figure 1A, B). The scales are nearly circular in shape with a mean diameter of 74.1 ± 11.2 μm (violet/deep blue: 58.3 ± 4.8 μm, N = 11; cyan/medium blue: 63.3 ± 7.1 μm, N = 22; green: 73.5 ± 6.1 μm, N = 17; orange/red: 84.1 ± 6.3 μm, N = 26) and generally feature a single intense, saturated hue (Figure 1B). At higher magnifications, however, the longer-wavelength reflecting scales show many smaller domains of different (smaller wavelength) hues.

2.2. Ultrastructure of the scales

We used scanning electron microscopy (SEM) to obtain real space information on the biophotonic nanostructures inside the scales (**Figure 2**). Figure 2A shows a single greenish-yellow wing scale with the enveloping cuticular cortex peeled off using a needle. Highly ordered polycrystallite domains of an apparent 3DPC with various orientations can be observed. High-magnification SEM images of a single domain of a blue-green and an orange-red scale are shown in Figure 2B and C, respectively. The crystallite *d*-spacing and consequently the lattice parameter can be readily seen to vary as expected between the latter two colors. As an exact determination of the topology and bulk structural information of 3DPCs is rather difficult using EM methods [38, 65], we performed synchrotron SAXS measurements.

2.3. Small-angle x-ray scattering (SAXS) of single scales

To structurally investigate the 3DPCs present in the iridescent rainbow-hued scales and ascertain their bulk structural parameters, we performed synchrotron SAXS assays. An individual red scale as well as on a piece of the elytron with an intact rainbow spot were systematically scanned in orthogonal directions to capture the ultrastructural basis of the color change (see **Figures 3** and **S1-S4**). The SAXS patterns from all scales examined exhibited a large number of discrete Bragg spots arrayed concentrically in the azimuthal direction (Figures 3A and S2A-E). This pattern is characteristic of a polycrystalline nanostructure and shows up to 8 orders of sharp diffraction spots (Figures 3B, C and S2F-J). This underscores the high

degree of long-range periodic order that is also apparent from the SEM images (Figure 2). Based on an indexing of these Bragg peaks as per IUCr crystallographic conventions [38, 42, 45, 66, 67] (Figures 3B, C and S2F-J), we identify the photonic nanostructure present in *P. c. pavonius* rainbow spot scales as belonging to the single diamond (*Fd*-3*m*) crystal symmetry, consistent with similarly diagnosed iridescent scales of other closely related Pachyrrhynchine weevils [42, 44, 45].

We observe no relationship between the width (FWHM) of the structural correlation peak scaled for the lattice dimensions (dq_{pk}/q_{pk}) or the corresponding ensemble-averaged polycrystallite domain or grain sizes (which can be approximated by the coherence length, $\xi \sim 2\pi/dq_{pk}$, expressed in μm) of the differently colored scales as a function of the peak position (Figures S3, S4). These results suggest that this weevil is able to intracellularly self-assemble single diamonds PCs at length scales across the visible spectrum with similar domain sizes. We measured an average crystallite domain size of 2.49 ± 0.23 μm (N = 6) across the multi-colored scales, which compares favorably with the EM data (Figure 2). The structure factor or correlation peak ranged from 0.0228 to 0.0260 nm^{-1} (corresponding to optical peaks at ~645 to 565 nm assuming an effective RI of 1.17 for the 3DPC; see below) for the scales assayed, with the peak shifting to smaller q values for scales reflecting a bathochromically shifted peak wavelength, as expected. Based on our SAXS nanostructural diagnoses combined with real space information, many of the polycrystallite domains of these single diamond PCs seem to be preferentially oriented with their <111> directions normal to the plane of the scale (Figure 2), similar to the preferential orientation documented in the 3DPCs of some iridescent butterfly wing scales [68-70].

2.4. Optical microspectrophotometry

To investigate the optical reflection properties of the rainbow-hued weevil scales, we performed microspectrophotometry on single wing scales, *i.e.*, we measured reflectance spectra from a

patch ~20 μm^2 using a diode spectrometer. The measured reflectance spectra differed strongly for the differently colored scales (**Figure 4**). The reflectance spectra were more or less single-peaked with peak wavelengths ranging across the entire visible wavelength range, between ~417-650 nm. However, the widths of these peaks are potentially confounded by multiple scattering of light [38] and local variation in polycrystalline domain orientations (see e.g. red scales in **Figure 1B**). By contrast to the SAXS structural data (Figure S3), the measured optical bandwidth (FWHM), scaled for the feature size or hue, significantly decreased with increasing spectral peak position or hue (**Figure S5**). This suggests that the longer wavelength structural colors are perhaps optically more saturated.

By matching the measured SAXS structural peak positions to the optical reflectance peaks, we estimated the effective RI of the 3DPCs (mean 1.17 ± 0.01, N = 6) and thus, the chitin volume or filling fractions (mean 0.345 ± 0.010, N = 6) by applying Maxwell-Garnett effective medium approximation theory [39, 71]. The chitin volume fractions significantly increased with increasing hue, indicating that the weevils are also using this parameter to tune their structural colors, in addition to varying the lattice parameters of the 3DPC.

2.5. Photonic bandgap modelling

The space group symmetries and orientation of a PC determines the photonic response to incident light. Generally, biological photonic crystals do not possess complete or full photonic bandgaps, owing to the relatively small RI contrast of organic dielectric material against air (the RI of chitin is ~1.56 [72, 73]). This implies that the orientation of the crystal and the resulting directional reflections arising from the corresponding pseudo bandgap become crucially important from a signaling perspective.

The elytral scales of *P.c. pavonius* range in color from blue to orange-red. The different colors obviously result from the interference of incident light by the single diamond PC and is modulated by varying both the chitin fill fraction and the unit cell size, as seen above. We

quantitatively explored the coloration strategy employed by this weevil by calculating the PBG diagrams for single diamond PCs with various different orientations and over a range of chitin filling fractions using the MIT photonic bands (MPB) software [74]. **Figure 5**A shows a map of the photonic stop bands for different high-symmetry directions Γ-L, Γ-X and Γ-U and different chitin filling fractions. The largest mid-gap to gap ratios occur at filling fractions of ~0.35-0.40, while smaller and larger filling fractions show increasingly marginal stop bands. Intriguingly, our estimated chitin filling fractions for the longer-wavelength reflecting scales (~0.36) are within this optimal range, whereas the green and blue (by interpolation) scales have filling fractions < 0.30 (see **Figure S6**). This explains why the scaled optical bandwidth ($\Delta\lambda/\lambda_{pk}$) decreases with increasing hue (Figure S5), as these longer-wavelength reflecting scales possess nanostructures with more or less optimal filling fractions to achieve maximal frequency midgap-gap ratio of the stop bands, which in turn increases the optical purity or saturation of the color [10]. Figure 5B shows how identical interference colors can be achieved by using different combinations of unit cell sizes and filling fractions, for comparison to the actual strategy employed by this weevil (also see **Figures S7** and **S8**).

3. Discussion

Quite a number of studies on insect biophotonic nanostructures, including Welch *et al*. [64] for the weevil *P. c. pavonius* examined in this study, have suggested that the control of the orientation of the polycrystallite domains (normal to the plane of the scale) is the usual strategy employed by nature to produce various different hues on the same animal [70, 75-79, but see 80]. Light interfering with these nanostructures usually results in a sort of pointillist color mixing in the far-field. Here, we have shown that *P. c. pavonius* employs a different strategy on a scale-by-scale basis. Both the lattice parameters and the chitin filling fractions of the 3DPC are varied to generate the rainbow-like spectrum of colors. This tuning of the structural

parameters of a complex 3DPC such as the single diamond to achieve a literal rainbow of colors on a scale-by-scale basis is unprecedented and quite remarkable for a biological system. A similar tuning of just the lattice parameter, albeit of a simple multilayer reflector, to produce a range of structural colors is known in the Madagascan sunset moth (*Chrysiridia rhipheus*) [81]. Interestingly, dynamically tunable biophotonic systems in (mainly marine) animals are also based on 1D multilayer reflectors but can involve changes in *d*- spacing as well as effective refractive index of the reflector, as in this weevil [82-87].

Incidentally, our systematic structural and optical analyses of the variously colored scales of the rainbow elytral spot has revealed some unexpected clues as to their development. The spatially monotonic changes in both scale color and scale diameter radially across the rainbow spot (Figures 1 and S1) as well as the decrease in chitin volume fraction with decreasing hue (Figure S6) appear to show a wavefront-like progression. This suggests that the duration and the rate of scale growth and chitin expression during development may determine the feature size and volume fraction of the nanostructure. At the same time, these results are consistent with a reaction-diffusion model of a morphogen gradient, perhaps one that is already implicated in the formation of spot-like features in insects [88, 89]. This gradient could also modulate differential chitin expression [90] and scale growth. Further transcriptomic and developmental studies on these interesting weevil 3DPC are sorely needed to address these tantalizing questions.

4. Conclusion

Using synchrotron SAXS, scanning electron microscopy, microspectrophotometry and photonic bandgap modeling, we conclude that iridescent scales present in the rainbow-hued spots on the elytra of the snout weevil, *P. c. pavonius* are due to a 3D photonic nanostructure with a single diamond network morphology of chitin in air. This weevil is varying both the

chitin filling fractions as well as the lattice parameter of the 3DPC to achieve the remarkable tunability of the structural colors on a scale-by-scale basis. Notably, single diamond PCs exhibit the largest full photonic bandgaps, compared to any other photonic nanostructure [14, 15]. Given that the synthesis of triply periodic minimal surface based bicontinuous network nanostructures at visible frequencies is currently difficult, weevil-derived single diamond PCs can be used as templates for high index dielectric infiltration or replicated using inorganic synthesis [34, 91, 92]. A more rewarding future direction would be to biomimic their templated intra-cellular self-assembly [38, 42, 43, 45] *in vitro*, in order to fabricate tunable mesophases for multi-functional applications in photonics or sensing.

5. Experimental Section

Samples: *Pachyrrhynchus congestus pavonius* (Heller 1921, Coleoptera: Curculionidae: Entiminae: Pachyrhynchini) weevils were bought commercially at 'Insect-Sale' (www.insectsale.com) and were originally collected in the Philippines.

Optical Microscopy and Microspectrophotometry: Reflectance of the elytral scales were measured with a microspectrophotometer: an adapted Zeiss Axioskop A1 with a fiber output connected to an Ocean Optics Maya LSL photodiode spectrometer. Light microscope pictures were acquired using a Point Grey Grasshopper 3 USB3 camera. A white diffusing reference tile (Ocean Optics WS-2) served as the reference in all spectroscopic measurements. Image analysis (FFT) was performed using ImageJ2 [93]. The unprocessed optical reflectance measurements were deconvolved or peak-fitted to estimate the relevant optical peak parameters such as wavelength of peak reflectance or hue, intensity or brightness and width (FWHM) or saturation of the reflectance peak using Fityk peak-fitting software as described elsewhere [39].

Electron Microscopy: Scanning electron microscopy (SEM) was performed using a Tescan Mira 3 field-emission SEM. To prevent charging effects, the samples were sputter-coated prior to imaging with a ~2 nm thin layer of gold or platinum.

Small angle X-ray scattering: Wing scales were sandwiched between 0.0025-inch (~63.5 μm) thick adhesive Kapton polyimide tape (McMaster-Carr catalogue no. 7648A33) for SAXS data collection. Pinhole SAXS (1.68 Å, 7.34 keV, 15 μm horizontal x 15 μm vertical beam, 50 x 0.5 s exposures, sample to detector distance 4 m) data in transmission geometry were collected at beamline 8-ID-I of the Advanced Photon Source, Argonne National Labs, Chicago, Illinois, USA from individual arthropod scales and processed using standard protocols [38, 42, 45, 67]. The azimuthally averaged profiles were deconvolved, or peak-fitted, to estimate the peak q values, and the widths (FWHM) of the scattering peaks, using Fityk [39].

Optical modelling: PBG diagrams for the single-network diamond photonic crystal in a face-centered cubic (*f.c.c.*) basis were simulated using the MIT photonics bandgap package (MPB, http://ab-initio.mit.edu/mpb) [74]. The dielectric matrix of the PC was generated using the level-set approximation for a single diamond structure [13]:

$$\cos z \sin(x + y) + \sin z \cos(x - y) = t, \quad (1)$$

where the threshold parameter, t, determines the filling fraction of the dielectric network. To simulate a dielectric single-network diamond structure, the dielectric function $f(x,y,z)$ was chosen such that the spatially varying RI at a given point in the unit cell, $n(x,y,z) = 1.56$ if $f(x,y,z) <= t$, and $n(x,y,z) = 1$, otherwise.

Supporting Information

Supporting Information is available from the Wiley Online Library or from the authors.

Acknowledgements

We are grateful to Doekele G. Stavenga for on-going support. This research was partly supported through the National Centre of Competence in Research "*Bio-Inspired Materials*" and the Ambizione program of the Swiss National Science Foundation SNF (168223) to BDW, and a UK Royal Society Newton Fellowship, Linacre College EPA Cephalosporin Junior Research Fellowship and Yale-NUS College funds to VS. VS is grateful to Dan Morse and the Institute for Collaborative Biotechnologies at University of California, Santa Barbara, for hosting and providing support during his sabbatical. SAXS data was collected at beamline 8-ID with the help of Suresh Narayanan and Alec Sandy of the Advanced Photon Source at Argonne National Labs, and supported by the U.S. Department of Energy, Office of Science, Office of Basic Energy Sciences, under Contract DE-AC02-06CH11357.

Received: ((will be filled in by the editorial staff))
Revised: ((will be filled in by the editorial staff))
Published online: ((will be filled in by the editorial staff))

References

1. Fox, H. M.; Vevers, G., *The nature of animal colors*. Macmillan: New York, **1960**.
2. Fox, D. L., *Animal Biochromes and Structural Colors*. University of California Press: Berkeley, CA, **1976**.
3. Vukusic, P.; Sambles, J. R., *Nature* **2003,** *424*, 852-855.
4. Kinoshita, S.; Yoshioka, S.; Miyazaki, J., *Rep.Prog. Phys.* **2008,** *71*, 076401.
5. Srinivasarao, M., *Chem. Rev.* **1999,** *1935-1961*.
6. Prum, R. O.; Quinn, T.; Torres, R. H., *J. Exp. Biol.* **2006,** *209*, 749-765.
7. Kreit, E.; Mathger, L. M.; Hanlon, R. T.; Dennis, P. B.; Naik, R. R.; Forsythe, E.; Heikenfeld, J., *J. R. Soc. Interface* **2012,** *10*, 20120601.
8. Gur, D.; Politi, Y.; Sivan, B.; Fratzl, P.; Weiner, S.; Addadi, L., *Angew. Chem. Int. Ed.* **2013,** *52* (1), 388-91.
9. Hecht, E., *Optics*. 2nd ed.; Addison-Wesley Publishing: Reading, Massachusetts, **1987**.
10. Joannopoulos, J. D.; Johnson, S. G.; Winn, J. N.; Meade, R. D., *Photonic crystals: Molding the flow of light*. 2nd ed.; Princeton University Press: New Jersey, **2008**.
11. Prum, R. O., Anatomy, physics, and evolution of avian structural colors. In *Bird Coloration, Volume 1 Mechanisms and Measurements*, Hill, G. E.; McGraw, K. J., Eds. Harvard University Press: Cambridge, MA, 2006; Vol. 1, pp 295-353.

12. Noh, H.; Liew, S. F.; Saranathan, V.; Mochrie, S. G. J.; Prum, R. O.; Dufresne, E. R.; Cao, H., *Adv. Mater.* **2010,** *22*, 2871-2880.
13. Wohlgemuth, M.; Yufa, N.; Hoffman, J.; Thomas, E. L., *Macromolecules* **2001,** *34*, 6083-6089.
14. Maldovan, M.; Urbas, A. M.; Yufa, N.; Carter, W. C.; Thomas, E. L., *Phys. Rev. B* **2002,** *65*, 165123.
15. Maldovan, M.; Ullal, C. K.; Carter, W. C.; Thomas, E. L., *Nat. Mater.* **2003,** *2*, 664-667.
16. Saba, M.; Thiel, M.; Turner, M. D.; Hyde, S. T.; Gu, M.; Grosse-Brauckmann, K.; Neshev, D. N.; Mecke, K.; Schroder-Turk, G. E., *Phys. Rev. Lett.* **2011,** *106*, 103902.
17. Guldin, S.; Docampo, P.; Stefik, M.; Kamita, G.; Wiesner, U.; Snaith, H. J.; Steiner, U., *Small* **2012,** *8*, 432-40.
18. Vignolini, S.; Yufa, N. A.; Cunha, P. S.; Guldin, S.; Rushkin, I.; Stefik, M.; Hur, K.; Wiesner, U.; Baumberg, J. J.; Steiner, U., *Adv. Mater.* **2012,** *24*, OP23-OP27.
19. Lu, L.; Fu, L.; Joannopoulos, J. D.; Soljacic, M., *Nat. Photon.* **2013,** *7*, 294-299.
20. Turner, M. D.; Saba, M.; Zhang, Q.; Cumming, B. P.; Schröder-Turk, G. E.; Gu, M., *Nat. Photon.* **2013,** *7*, 801-805..
21. Dolan, J. A.; Wilts, B. D.; Vignolini, S.; Baumberg, J. J.; Steiner, U.; Wilkinson, T. D., *Adv. Opt. Mater.* **2015,** *3*, 12-32.
22. Stefik, M.; Guldin, S.; Vignolini, S.; Wiesner, U.; Steiner, U., *Chem. Soc. Rev.* **2015,** *44*, 5076-91.
23. Hajduk, D. A.; Harper, P. E.; Gruner, S. M.; Honeker, C. C.; Kim, G.; Thomas, E. L.; Fetters, L. J., *Macromolecules* **1994,** *27*, 4063-4075.
24. Matsen, M. W.; Carlo, M.; Block, I.; Saxs, U., *Physics* **1998,** *108*, 785-796.
25. Bates, F. S.; Fredrickson, G. H., *Phys. Today.* **1999,** *52*, 32-38.
26. Fink, Y.; Urbas, A. M.; Bawendi, M. G.; Joannopoulos, J. D.; Thomas, E. L., *J. Lightwave Technol.* **1999,** *17*, 1963-1969.
27. Thomas, E. L.; Urbas, A.; Sharp, R.; Fink, Y.; Xenidou, M.; Fetters, L. J., *Adv. Mater.* **2000,** *12*, 812-814.
28. Urbas, B. A. M.; Maldovan, M.; Derege, P.; Thomas, E. L., *Adv. Mater.* **2002,** *14*, 1850-1853.
29. Epps, T. H.; Cochran, E. W.; Hardy, C. M.; Bailey, T. S.; Waletzko, R. S.; Bates, F. S., *Macromolecules* **2004,** *37*, 7085-7088.
30. Kang, Y.; Kang, C.; Kim, E.; Baek, H.; Hwang, K.; Kwak, D.; Thomas, E. L., *J. Am. Chem. Soc.* **2009,** *131*, 7538.
31. Gan, Z. S.; Turner, M. D.; Gu, M., *Sci. Adv.* **2016,** *2*, e1600084.
32. Ullal, C. K.; Maldovan, M.; Thomas, E. L.; Chen, G.; Han, Y. J.; Yang, S., *Appl. Phys. Lett.* **2004,** *84*, 5434.
33. Galusha, J. W.; Richey, L. R.; Jorgensen, M. R.; Gardner, J. S.; Bartl, M. H., *J. Mater. Chem.* **2010,** *20*, 1277-1284.
34. Mille, C.; Tyrode, E. C.; Corkery, R. W., *RSC Adv.* **2013,** *3*, 3109-3117.
35. Arnold, J. M., *J. Ultrastruct. Res.* **1967,** *20*, 410-21.
36. Ghiradella, H., *J. Morphol.* **1989,** *202*, 69-88.
37. Prum, R. O.; Dufresne, E. R.; Quinn, T.; Waters, K., *J. R. Soc. Interface* **2009,** *6*, S253-S265.
38. Saranathan, V.; Osuji, C. O.; Mochrie, S. G. J.; Noh, H.; Narayanan, S.; Sandy, A.; Dufresne, E. R.; Prum, R. O., *P. Natl. Acad. Sci. USA* **2010,** *107*, 11676-11681.
39. Saranathan, V.; Forster, J. D.; Noh, H.; Liew, S. F.; Mochrie, S. G. J.; Cao, H.; Dufresne, E. R.; Prum, R. O., *J. R. Soc. Interface* **2012,** *9*, 2563–2580.
40. Maia, R.; Macedo, R. H.; Shawkey, M. D., *J. R. Soc. Interface* **2012,** *9*, 734-43.

41. DeMartini, D. G.; Krogstad, D. V.; Morse, D. E., *Proc. Natl. Acad. Sci. USA* **2013,** *110*, 2552-2556.
42. Saranathan, V.; Seago, A. E.; Narayanan, S.; Sandy, A.; Mochrie, S. G. J.; Dufresne, E. R.; Cao, H.; Osuji, C. O.; Prum, R. O., *Nano Lett.* **2015,** *15*, 3735-42.
43. Wilts, B. D.; Apeleo Zubiri, B.; Klatt, M. A.; Butz, B.; Fischer, M. G.; Kelly, S. T.; Spiecker, E.; Steiner, U.; Schroder-Turk, G. E., *Sci. Adv.* **2017,** *3*, e1603119.
44. Seago, A. E.; Saranathan, V., Photonic Crystals in Beetles. In *Nature's Nanostructures*, Pan Stanford Publishing: 2012; pp 313-326.
45. Saranathan, V., Topology of minimal surface biophotonic nanostructures in arthropods. In *Springer Series in Solid-State Sciences: The Role of Topology in Materials*, Gupta, S.; Saxena, A., Eds. Springer: New York, 2018; pp 275-290.
46. Leertouwer, H. L.; Wilts, B. D.; Stavenga, D. G., *Opt. Exp.* **2011,** *19*, 24061-24066.
47. Stavenga, D. G.; Leertouwer, H.; Wilts, B. D., *Light Sci. Appl.* **2013,** *2*, e100.
48. Wilts, B. D.; Wijnen, B.; Leertouwer, H. L.; Steiner, U.; Stavenga, D. G., *Adv. Opt. Mater.* **2017,** *5*, 1600879.
49. Zi, J.; Yu, X.; Li, Y.; Hu, X.; Xu, C.; Wang, X.; Liu, X.; Fu, R., *Proc. Natl. Acad. Sci. USA* **2003,** *100*, 12576-12578.
50. Hallam, B. T.; Hiorns, A. G.; Vukusic, P., *Appl. Optics* **2009,** *48* (17), 3243-3249.
51. Pouya, C.; Vukusic, P., *Interface focus* **2012,** *2*, 645-650.
52. Yin, H.; Dong, B.; Liu, X.; Zhan, T.; Shi, L.; Zi, J.; Yablonovitch, E., *Proc. Natl. Acad. Sci. USA* **2012,** *109*, 10798-801.
53. Burresi, M.; Cortese, L.; Pattelli, L.; Kolle, M.; Vukusic, P.; Wiersma, D. S.; Steiner, U.; Vignolini, S., *Sci. Rep.* **2014,** *4*, 6075.
54. Wilts, B. D.; Sheng, X.; Holler, M.; Diaz, A.; Guizar-Sicairos, M.; Raabe, J.; Hoppe, R.; Liu, S. H.; Langford, R.; Onelli, O. D.; Chen, D.; Torquato, S.; Steiner, U.; Schroer, C. G.; Vignolini, S.; Sepe, A., *Adv. Mater.* **2018**, *30*, 201702057.
55. Schroeder, T. B. H.; Houghtaling, J.; Wilts, B. D.; Mayer, M., *Adv. Mater.* **2018,** *30* , 201705322.
56. Biro, L. P.; Vigneron, J. P., *Laser Photon. Rev.* **2011,** *5*, 27-51.
57. Parker, A. R.; Townley, H. E., *Nat. Nanotechnol.* **2007,** *2*, 347-353.
58. Seago, A. E.; Brady, P.; Vigneron, J.-P.; Schultz, T. D., *J. R. Soc Interface* **2009,** *6*, S165-S184.
59. Stavenga, D. G.; Wilts, B. D.; Leertouwer, H. L.; Hariyama, T., *Philos. Trans. R. Soc. B* **2011,** *366*, 709-723.
60. Sharma, V.; Crne, M.; Park, J. O.; Srinivasarao, M., *Science* **2009,** *325*, 449-451.
61. Wilts, B. D.; Whitney, H. M.; Glover, B. J.; Steiner, U.; Vignolini, S., *Mater. Tod. Proc.* **2014,** *1*, 177-185.
62. Parker, A. R.; Welch, V. L.; Driver, D.; Martini, N., *Nature* **2003,** *426*, 786-787.
63. Galusha, J. W.; Richey, L. R.; Gardner, J. S.; Cha, J. N.; Bartl, M. H., *Phys. Rev. E* **2008,** *77*, 2-5.
64. Welch, V.; Lousse, V.; Deparis, O.; Parker, A.; Vigneron, J. P., *Phys. Rev. E* **2007,** *75*, 1-9.
65. Argyros, A.; Large, M. C. J.; McKenzie, D. R.; Cox, G. C.; Dwarte, D. M., *Micron* **2002,** *33*, 483-487.
66. Hahn, T., The 230 space groups. In *IUCr International Tables for Crystallography* Springer: 2006; Vol. A, Ch. 7.1, pp 112-717.
67. McNamara, M. E.; Saranathan, V.; Locatelli, E. R.; Noh, H.; Briggs, D. E.; Orr, P. J.; Cao, H., *J. R. Soc. Interface* **2014,** *11*, 20140736.
68. Singer, A.; Boucheron, L.; Dietze, S. H.; Jensen, K. E.; Vine, D.; McNulty, I.; Dufresne, E. R.; Prum, R. O.; Mochrie, S. G.; Shpyrko, O. G., *Sci. Adv.* **2016,** *2*, e1600149.

69. Yoshioka, S.; Fujita, H.; Kinoshita, S.; Matsuhana, B., *Journal of the Royal Society Interface* **2014,** *11*, 20131029.
70. Corkery, R. W.; Tyrode, E. C., *Interface focus* **2017,** *7*, 20160154.
71. Forster, J. D.; Noh, H.; Liew, S. F.; Saranathan, V.; Schreck, C. F.; Yang, L.; Park, J. G.; Prum, R. O.; Mochrie, S. G. J.; O'Hern, C. S.; Cao, H.; Dufresne, E. R., *Adv. Mater.* **2010,** *22*, 2939-2944.
72. Vukusic, P.; Sambles, J. R.; Lawrence, C. R.; Wootton, R. J., *Proc. R. Soc. B* **1999,** *266*, 1403-1411.
73. Yoshioka, S.; Kinoshita, S., *Phys. Rev. E* **2011,** *83*, 051917.
74. Johnson, S.; Joannopoulos, J., *Opt. Express* **2001,** *8*, 173-190.
75. Pouya, C.; Stavenga, D. G.; Vukusic, P., *Opt. Express* **2011,** *19*, 11355-11364.
76. Wilts, B. D.; Michielsen, K.; Kuipers, J.; De Raedt, H.; Stavenga, D. G., *Proc. R. Soc. B* **2012,** *279*, 2524-2530.
77. Mouchet, S.; Colomer, J. F.; Vandenbem, C.; Deparis, O.; Vigneron, J. P., *Opt. Express* **2013,** *21*, 13228-13240.
78. Wilts, B. D.; Ijbema, N.; Michielsen, K.; De Raedt, H.; Stavenga, D. G., *MRS Proc.* **2013,** *1504*, mrsf12-1504-v08-03.
79. Wu, X.; Erbe, A.; Raabe, D.; Fabritius, H.-O., *Adv. Funct. Mater.* **2013,** *23*, 3615-3620.
80. Nagi, R. K.; Montanari, D. E.; Bartl, M. H., *Bioinspir. Biomim.* **2018,** *13*, 035003.
81. Yoshioka, S.; Nakano, T.; Nozue, Y.; Kinoshita, S., *J. R. Soc. Interface* **2008,** *5*, 457-464.
82. Kasukawa, H.; Oshima, N., *Pigment Cell Res.* **1987,** *1* (3), 152-157.
83. Mäthger, L. M.; Land, M. F.; Siebeck, U. E.; Marshall, N. J., *J. Exp. Biol.* **2003,** *206*, 3607-3613.
84. Vigneron, J. P.; Pasteels, J. M.; Windsor, D. M.; Vértesy, Z.; Rassart, M.; Seldrum, T.; Dumont, J.; Deparis, O.; Lousse, V.; Biró, L. P.; Ertz, D.; Welch, V., *Phys. Rev. E* **2007,** *76*, 1-10.
85. Tao, A. R.; DeMartini, D. G.; Izumi, M.; Sweeney, A. M.; Holt, A. L.; Morse, D. E., *Biomaterials* **2010,** *31*, 793-801.
86. Rassart, M.; Simonis, P.; Bay, A.; Deparis, O.; Vigneron, J. P., *Phys. Rev. E* **2009,** *80*, 031910.
87. Izumi, M.; Sweeney, A. M.; Demartini, D.; Weaver, J. C.; Powers, M. L.; Tao, A.; Silvas, T. V.; Kramer, R. M.; Crookes-Goodson, W. J.; Mathger, L. M.; Naik, R. R.; Hanlon, R. T.; Morse, D. E., *J. R. Soc. Interface* **2010,** *7*, 549-560.
88. Nijhout, H. F., *Proc. R. Soc. B* **1990,** *239*, 81-113.
89. Nijhout, H. F., *The Development and Evolution of Butterfly Wing Patterns*. Smithsonian Institution Press: Washington, **1991**; p 297.
90. Wang, P.; Qiu, Z.; Xia, D.; Tang, S.; Shen, X.; Zhao, Q., *PloS one* **2017,** *12*, e0175994.
91. Weatherspoon, M. R.; Cai, Y.; Crne, M.; Srinivasarao, M.; Sandhage, K. H., *Angew. Chem. Int. Ed.* **2008,** *47*, 7921-7923.
92. Galusha, J. W.; Jorgensen, M. R.; Bartl, M. H., *Adv. Mater.* **2010,** *22*, 107-110.
93. Rueden, C. T.; Schindelin, J.; Hiner, M. C.; DeZonia, B. E.; Walter, A. E.; Arena, E. T.; Eliceiri, K. W., *BMC Bioinformatics* **2017,** *18* (1), 529.

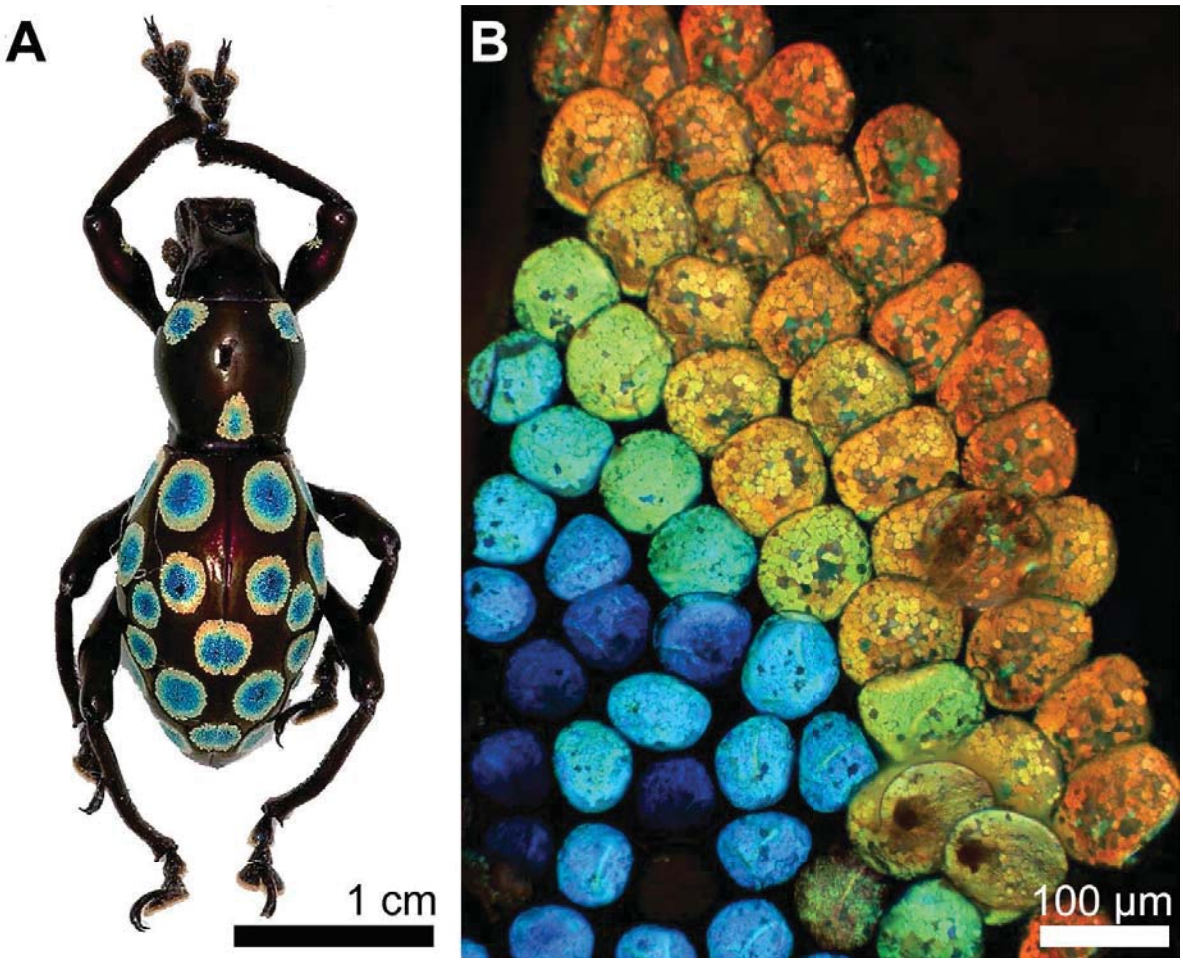

Figure 1. The "Rainbow" Weevil, *Pachhyrhynchus congestus pavonius*.
(**A**) Habitus photograph of the whole weevil. The elytra as well as the thorax are dotted with annular rainbow-colored spots. (**B**) A bright-field light microscope close-up image of the rim of a single elytral rainbow spot. The spot is composed of nearly circular scales or setae arranged in concentric rings of different hues, ranging from blue in the center to red at the outside, just like in a rainbow. Note, the size of the scales get progressively smaller going from red to blue radially inwards.

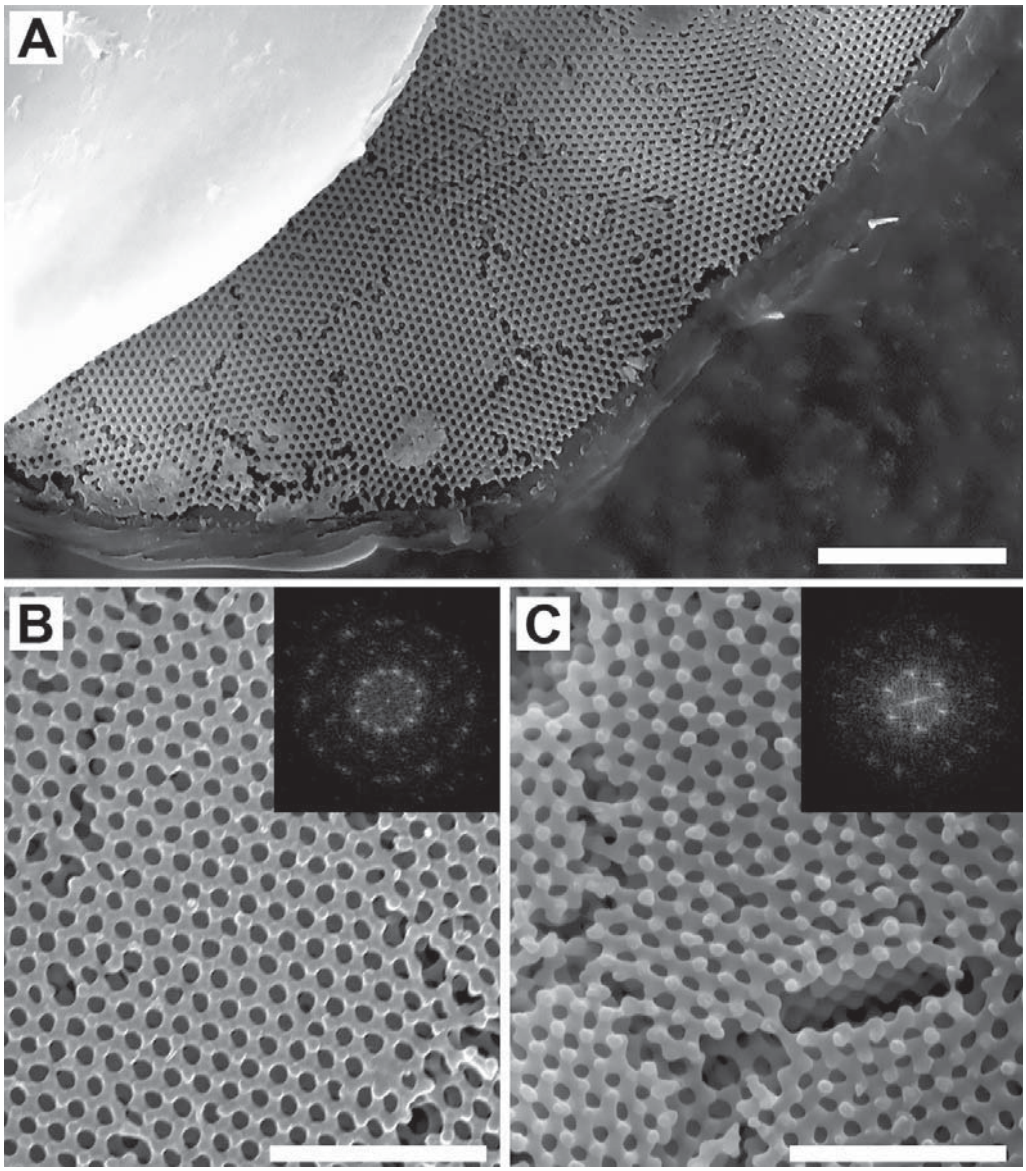

Figure 2. Ultrastructure of the wing scales of *P. c. pavonius*.
(**A**) SEM image of a single green-colored scale with the enveloping outer cortex peeled off. Several different polycrystallite domains of the 3DPC are discernible, but notably nearly all domains seem to exhibit roughly the same *<111>* orientation of the single diamond 3DPC, normal to the plane of the scale. (**B**, **C**) Close-up SEM images of a single domain from a (**B**) blue-green and (**C**) orange-red wing scale. Scale bars: (**A**) 5 μm, (**B**, **C**) 2 μm. Inset: FFT analyses of the micrographs of panels **B** and **C** give *d*-spacings of 239 ± 20 and 279 ± 30 nm, respectively.

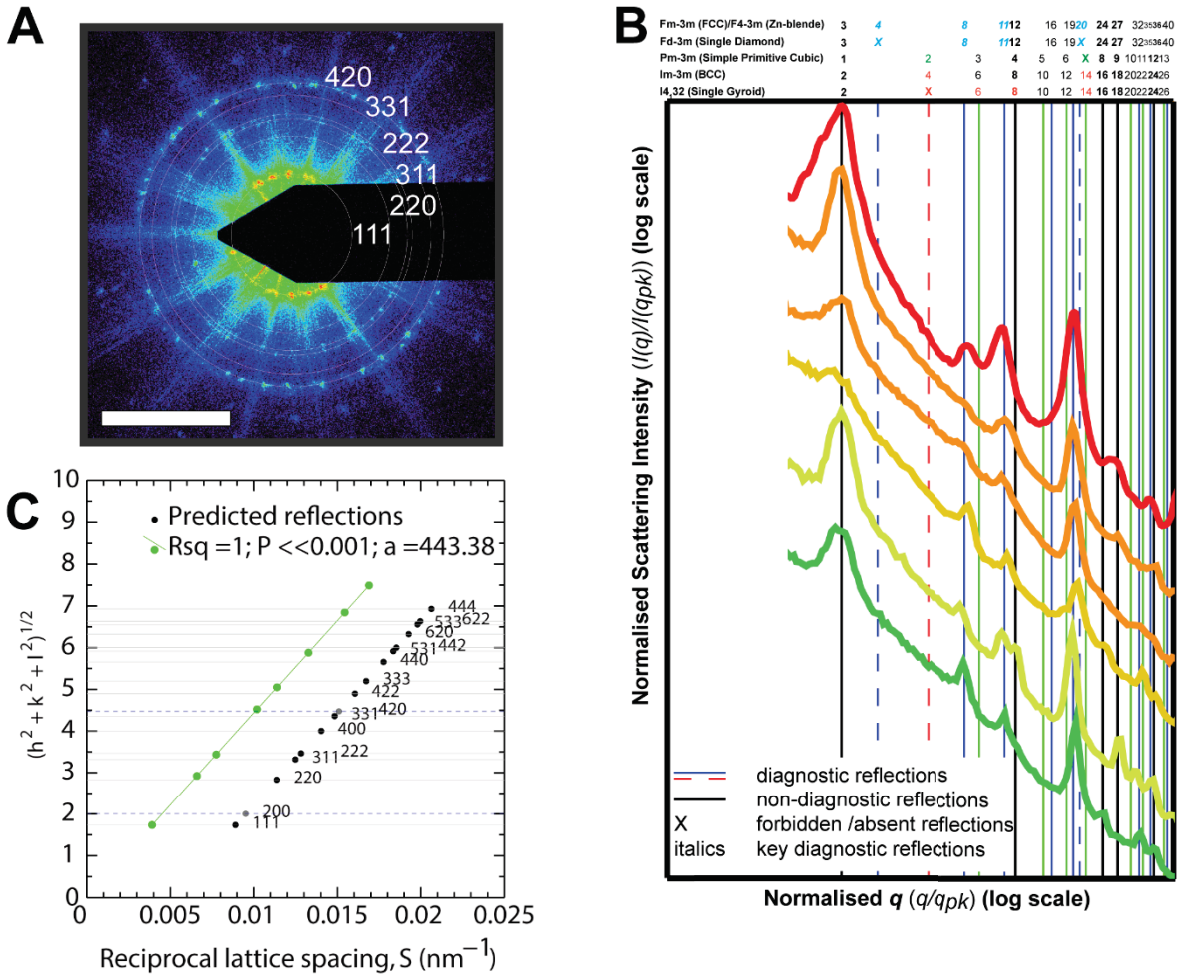

Figure 3: Synchrotron Small Angle X-ray Scattering (SAXS) structural analyses of rainbow spot scales of *P. c. pavonius*.

(**A**) A representative SAXS diffraction pattern from a rainbow spot scale, shown unmasked in false color and logarithmic scaling. The radii of the concentric circles are given by the peak scattering wave vector (q_{pk}) times the moduli of the assigned *hkl* indices of permitted Bragg reflections of a single diamond space-group. Scale bar: 0.05 nm^{-1}. (**B**) Normalized, azimuthally averaged SAXS profiles calculated from the respective 2D SAXS patterns (in Figs. 3A and S2 A-E) shown on a log-log scale. The colors of the lines correspond to the approximate hues of the scale, assuming an average RI of 1.17 for the corresponding 3DPC. The colored vertical lines correspond to the expected Bragg peak positional ratios for various alternative crystallographic space groups, presented together for direct comparison. The numbers above the vertical lines are squares of the moduli of the Miller indices (*hkl*) for the allowed reflections of specific space-groups. (**C**) Indexing the peaks of the azimuthally averaged profile of the SAXS pattern in Figure S2B, using the plot of the moduli of the *hkl* Miller indices of the Bragg peaks against the corresponding reciprocal lattice spacing *S*. The observed peaks (solid green circles) are shown alongside the theoretically allowed reflections for the single diamond (*Fd-3m*; black circles) and f.c.c. (*F*4-3*m*; gray + black circles) crystallographic space group symmetries. The linearity and zero intercepts of the plot confirm the cubic aspect of the nanostructure, and the slope gives an estimate of the lattice parameter.

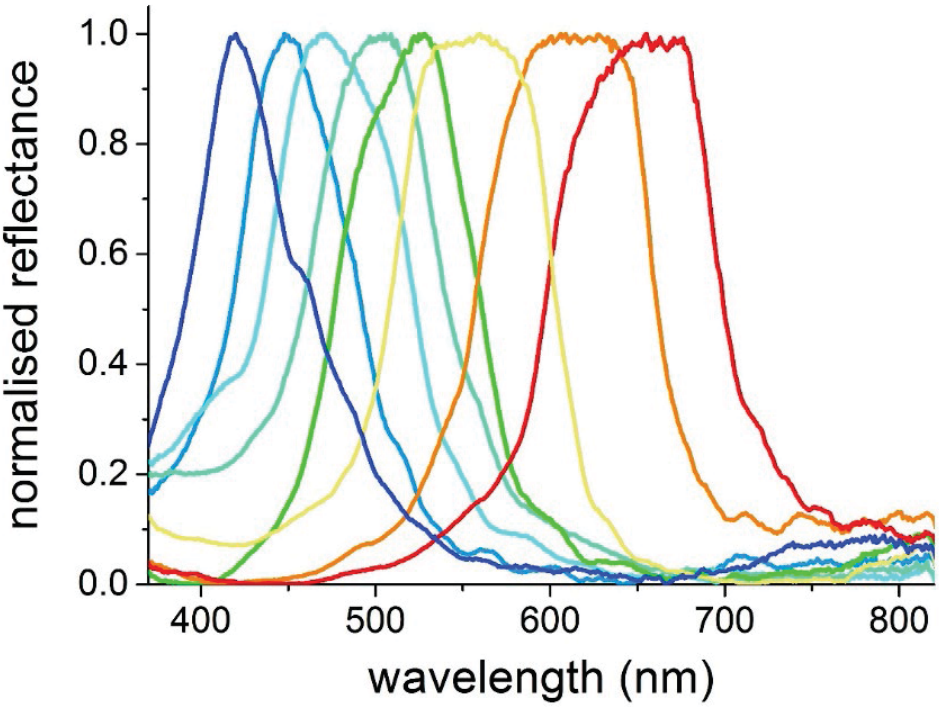

509

510 **Figure 4: Normalized reflectance spectra of single scales of various hues measured**
511 **by microspectrophotometry.**

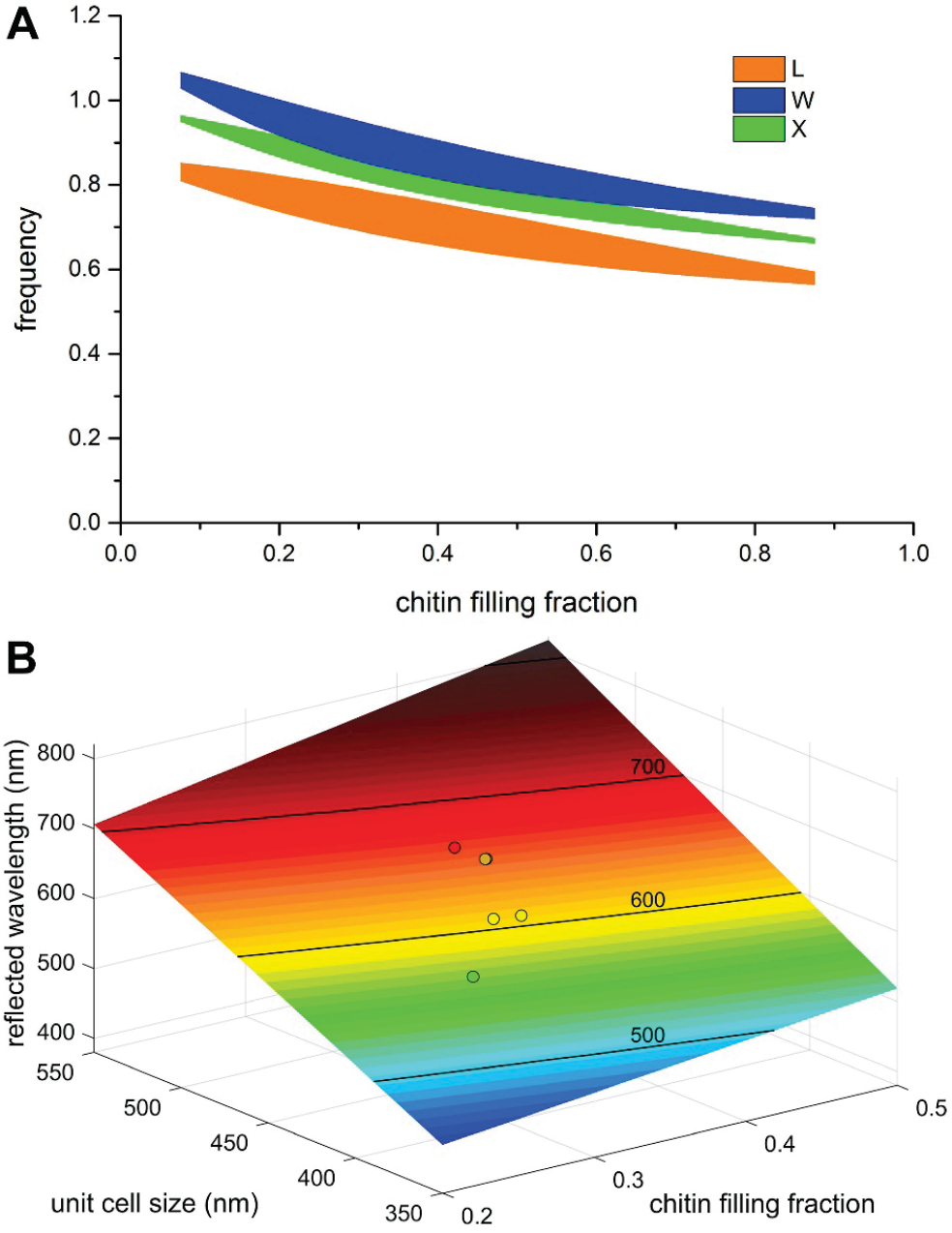

Figure 5: Photonic bandgap modelling.
(**A**) Frequency-dependent bandgap map for the three main high symmetry directions of a single-diamond PC, shown here as a function of chitin filling fraction. (**B**) Peak wavelength dependency of the unit cell size a and the chitin filling fraction ϕ in an Γ-L or [*111*] oriented single diamond PC. The SAXS measured lattice dimensions of assayed scales (N = 6) are shown overlaid, in order to estimate the approximate filling fractions.

3D nanostructured chitinous biomaterials are the basis of the iridescent colors of many insects. The study shows how the key parameters of a 3D single diamond network photonic crystal is tuned in the rainbow-colored wing scales of a weevil in order to achieve vivid iridescent colors that span the full visible wavelength range.

Biophotonics

B.D. Wilts* and V. Saranathan*

A literal elytral rainbow: Tunable structural colors using single diamond biophotonic crystals in *Pachyrrhynchus congestus* weevils